

GT2011-4) ' \$)

## EXPERIMENTAL CHARACTERIZATION OF LOW NO<sub>x</sub> MICROMIX PROTOTYPE COMBUSTORS FOR INDUSTRIAL GAS TURBINE APPLICATIONS

**H. H.-W. Funke**

Aachen University of Applied Sciences  
Aachen, Germany

**W. Krebs**

Siemens AG  
Energy Sector Fossil Power Generation Division  
Muelheim an der Ruhr, Germany

**S. Boerner**

Aachen University of Applied Sciences  
Aachen, Germany

**E. Wolf**

Siemens AG  
Energy Sector Technology & Innovation  
Erlangen, Germany

### ABSTRACT

The use of renewable discontinuous energy sources, such as wind- or solar-energy, raises the question of ensuring the continuous demand for energy. For future energy storage scenarios, hydrogen combustion systems play an important role. This offers new opportunities for alternative combustion processes with regard to efficient, safe and low NO<sub>x</sub> combustion of hydrogen. In addition hydrogen combustion technology will be in need of gas turbine technology for future IGCC power plant concepts.

Against the background of ensuring a secure and low NO<sub>x</sub> combustion of hydrogen, the micromix burning principle is developed since years and was first investigated for the use in aircraft jet engines to significantly reduce NO<sub>x</sub>-emissions. This combustion principle is based on cross-flow mixing of air and gaseous hydrogen and burns in multiple miniaturized diffusion-type flames. The two advantages of this principle are the inherent safety against flash back and the low NO<sub>x</sub>-emissions due to a very short residence time of reactants in the flame region of the micro-flames.

The paper presents an experimental in depth analysis of the combustion principle with regards to low NO<sub>x</sub>-emissions for higher energy densities. Therefore several geometric variations were investigated and the burning principle was scaled and tested for higher energy densities up to 15 MW/(m<sup>2</sup>bar). For the different geometries and energy densities, combustion stability, flame anchoring behavior and associated NO<sub>x</sub>-emissions are tested under preheated atmospheric conditions.

The experimental results show the successful scaling of the micromix principle for high energy densities. The general mapping of the test burners demonstrates a wide operating range. Flow phenomena influencing the flame lifting and flame

anchoring position with respect to the resulting NO<sub>x</sub>-emission are analyzed. The investigations highlight further potential for NO<sub>x</sub>-reduction in industrial gas turbine applications.

### 1. INTRODUCTION

In future electrical power supply scenarios, gas turbines will play an important role. Gas turbines are efficient, reliable, scalable and long-life energy systems. With the change to hydrogen as utilized fuel, the aspect of renewable energy sources can be integrated into gas turbine applications. In addition large scale Hydrogen energy storage systems in conjunction with industrial gas turbine power plant applications can be used in order to transfer renewable discontinuous energy sources into a continuous power supply [1].

The utilization of the IGCC power plant technology enables the combination of low cost coal and opportunity fuels, such as biomass, with the international effort to reduce the environmental impact of electricity generation, especially CO<sub>2</sub>-emissions, to cost effective future power plant systems. The high hydrogen content of the gases requires hydrogen combustion technology for the gas turbine operation of the IGCC power plant [2].

By using hydrogen as fuel for industrial gas turbine applications, with regard to the hydrogen's unique combustion properties, the question arises, how the hydrogen can be burned stable and efficient with minimum possible NO<sub>x</sub>-emissions. The first investigations of the application of hydrogen as fuel for gas turbines are carried out for aero engines in the 1950's and were mostly supported by military considerations [3,4]. After the oil crisis, the thought of using hydrogen as a possible alternative fuel, with only NO<sub>x</sub>-emissions as pollutants, for aero engines came to the fore [5]. A lot of research work was done

on the topic of low NO<sub>x</sub> hydrogen combustion and the development of conception-design of a hydrogen operated airplane during the research programs EQHHPP [6] and CRYOPLANE [7] in the 1990's as far as to the year 2000.

The research work on industrial hydrogen operated gas turbines for power plant application is mostly driven by the vision to implement IGCC-Technology into power plant design [2, 8, 9] and to use the Hydrogen as large scale energy storage for renewable sources. In addition to the investigations on hydrogen fuelled gas turbines [10], several design studies [11] are carried out in order to develop a low NO<sub>x</sub> hydrogen combustor.

The research activities on the Aachen University of Applied Sciences arise from the European research projects EQHHPP and CRYOPLANE. In the framework of these research activities the micromix burning principle was invented and investigated for the use of gaseous hydrogen as fuel in aircraft jet engines to significantly reduced NO<sub>x</sub>-emissions [12]. For these investigations an Auxiliary Power Unit as test rig gas turbine is used. The combustion chamber based on the micromix burning principle for the integration in the APU GTCP 36-300 has an energy density of 5.73 MW/(m<sup>2</sup>bar). A review of the previous research activities is presented in [13].

In the year 2008 Aachen University of Applied Sciences and Siemens AG decided to investigate the ability of the micromix burning principle for higher energy density industrial gas turbine applications. Three energy densities were chosen for the experimental investigations. Starting with a 5 MW/(m<sup>2</sup>bar)-reference system the burning principle is scaled up to an energy density of 15 MW/(m<sup>2</sup>bar). Especially the resultant NO<sub>x</sub>-emissions with increased energy density are of major interest.

## 2. MICROMIX BURNING PRINCIPLE

When using conventional combustors in hydrogen fuelled gas turbines high NO<sub>x</sub>-emissions result [12]. In order to avoid environmental pollution and to meet legal standards the combustion process has to be modified with regard to low NO<sub>x</sub>-emissions. NO<sub>x</sub>-emissions include NO<sub>2</sub> and NO. Which one is the main component on the total NO<sub>x</sub>-formation is dependent on the combustion process. The possible formation routes and their characteristics are still part of current research activities. An intensive review of these research activities, especially against the background of the combustion of hydrogen in industrial gas turbines, is presented in [14].

In [15] Lefebvre suggests that the NO<sub>x</sub>-formation is determinate by three influence parameters: reaction rate, residence time and mixture. Reaction rate includes all prevailing ambient conditions, i.e. temperature and pressure, during the combustion process. For gas turbine operations these parameters are given by the gas turbine's cycle conditions. Shifting these parameters for lowering the NO<sub>x</sub>-formation decreases the gas turbine's efficiency. But a formation of hot spots in the combustion chamber has to be avoided.

Enhancing the mixing seems to be one of the promising ways in lowering NO<sub>x</sub>-formation [16]. Premixed hydrogen combustion principles show good reduction potential [17]. For

premixed systems the risk of flash back has to keep in mind during operation under gas turbine conditions due to the hydrogen's high reactivity and flame velocity. By using non premixed systems the question appears how the mixture can be enhanced in order to limit increased formation rates. For increasing the mixture, the fluid mechanic phenomenon of jets in cross-flow is used by the micromix burning principle (Figure 1a). For the characterization of the jet in cross-flow the momentum ratio  $r_m$  is used and defined as [18]:

$$r_m = \sqrt{\frac{\rho_j * u_j^2}{\rho_\infty * u_\infty^2}} \quad (1)$$

In which  $\rho_j$  and  $u_j$  are the density and the velocity of the injected jet. In case of the micromix burning principle it is the density and the velocity of the injected hydrogen mass flow.  $\rho_\infty$  and  $u_\infty$  are the density and the velocity of the surrounding air flow. The injection depth of the hydrogen into the air flow is defined as [18]:

$$y_{max} = (1 - 2) * d_j * r_m \quad (2)$$

The term  $d_j$  is the diameter of the hydrogen injection hole. After the cross-flow interaction the hydrogen burns as a diffusion type flame.

With reference to [15] the remaining parameter influencing NO<sub>x</sub>-formation is the residence time. An increased residence time of reactants in the hot flame region results in higher NO<sub>x</sub>-formation [16]. Due to the hydrogen's high reaction rate it is possible to lower the residence time by separating the reaction zone into multiple micro diffusion flamelets instead of several large scale flames. Following this idea the design of the burner is governed by the need to distribute the hydrogen prior to injection across the entire main flow area to as many injection points as possible [12,13]. Through the miniaturization of the injection diameter the flame is miniaturized, too. The usage of miniaturized flames enhances also the mixing of the reactants. In summary the significant NO<sub>x</sub>-reduction potential of the micromix burning principle is based on the number and miniaturization of the H<sub>2</sub>-flames. Therewith the mixing between hydrogen and air is enforced while the residence time of reactants in the hot flame region is decreased due to the shortened flame length. Figure 1 (a,b) shows the resultant design of the micromix burning principle.

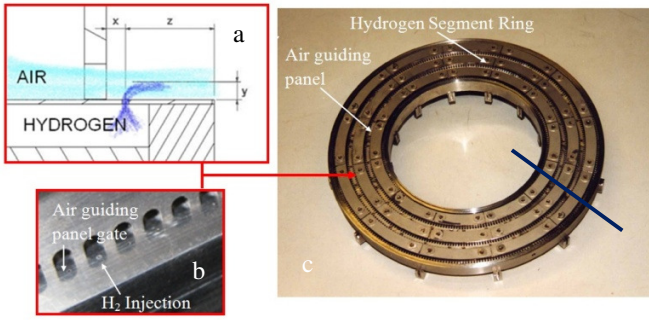


**Figure 1: The micromix burning principle**

Every  $H_2$  injection hole is attributed to an air guiding panel gate. So every “gate-injection hole”-combination represents a separate jet in cross-flow process (Figure 1a, b). The latest manufactured combustion chamber for the APU (Figure 1c) counts nearly 1600 miniaturized flames and has a thermal power of 1.6 MW. The main parts of the combustion chamber are the air guiding panels and the spoke centred hydrogen segment rings with the injection holes arranged on the ring. The blue line in Figure 1 indicates the cross-section of the combustion chamber. The cross-section and the recirculation zones resulting from burner geometry are presented in Figure 2.

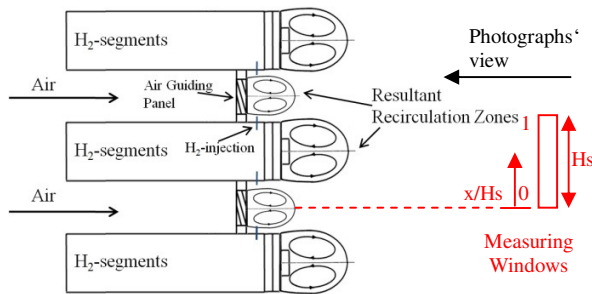


**Figure 2: Resultant Recirculation zones**

The dimension of the recirculation zones is based on the investigations by Beér and Davis [19] for the resultant wake formation of discs. For the micromix burning principle the flame anchoring is influenced by the formation of the recirculation zones as discussed later on.

### 3. SCALING OF THE MICROMIX COMBUSTION PRINCIPLE TO HIGHER ENERGY DENSITIES

The energy density is a dimension for the energy amount

**Table 1: Geometry Parameters**

Energy Density [MW/(m <sup>2</sup> bar)]	d <sub>H<sub>2</sub></sub> -Hole [mm]	H <sub>2</sub> mass flow per hole [g/h]	Injection depth y [mm]	Geometry air guiding panel	Distance H <sub>2</sub> injection holes [mm]
5	0.3	Reference = 3.23	Reference = 0.51		2.3
10	0.5	2.7 Reference	1.7 Reference		3.2
10	0.5	2.7 Reference	1.7 Reference		3.2
15	0.7	5.1 Reference	2.4 Reference		4.1

requested by the cycle conditions for ensuring the desired operational conditions under consideration of the available design space and the prevailing pressure conditions. As reference for the up scaling of the micromix burning principle to large scale industrial gas turbine applications the APU-reference system is used. This reference-system was also used for the successful downscaling of the micromix burning principle for  $\mu$ -scale hydrogen fuelled gas turbines [20]. The chosen scaling parameter for the up scaling is the energy density.

$$ED = \frac{\dot{m}_{H_2} * Hu_{H_2}}{A_{design\ space} * p_3} \quad ED = \left[ \frac{MW}{m^2\ bar} \right] \quad (3)$$

For the investigation of the energy density’s impact on the NO<sub>x</sub>-formation three different burner configurations, 5 MW/(m<sup>2</sup>bar), 10 MW/(m<sup>2</sup>bar) and 15 MW/(m<sup>2</sup>bar) are tested. The 5 MW/(m<sup>2</sup>bar)-configuration is the reference system for comparison with the two up scaled burner configurations.

Each “gate-injection hole”-combination represents a single jet in cross-flow process. By allocating the required numbers of flames the designated thermal energy can be achieved. But if the design space is limited and higher thermal energy amount is requested the energy density has to be enhanced. This can be reached by increasing the number of flames positioned in a decided area. But thereby the risk of flame merging exists. By keeping all major design parameters constant, i.e. momentum ratio, air and hydrogen exit velocities, the H<sub>2</sub> injection diameter has to be increased in order to have more injected energy per hole at the available design space. For preventing flame merging the distance between has to be increased. In consequence the hydrogen mass flow rate per hole and therewith the injection diameter has to be further increased due to the reduced design space. In addition the dimension of the air guiding panel gates has also to be adopted in order to keep the momentum ratio and exit velocities constant at the design point. Table 1 shows the resultant geometry parameters. Introducing a new design approach for the 10 MW/(m<sup>2</sup>bar)-configuration a gap-system instead of gate-configuration for the air guiding panels is tested.

### 4. EXPERIMENTAL SETUP

For the experimental investigation test burners are used. All tests were carried out at the atmospheric test rig at comparable inlet conditions. The air is preheated up to the

APU's specific inlet temperature of 560K. The pressurized design point of the APU GTCP 36-300 is scaled by similarity of the Mach number to atmospheric conditions. Figure 3 shows a test burner mounted on the test rig.

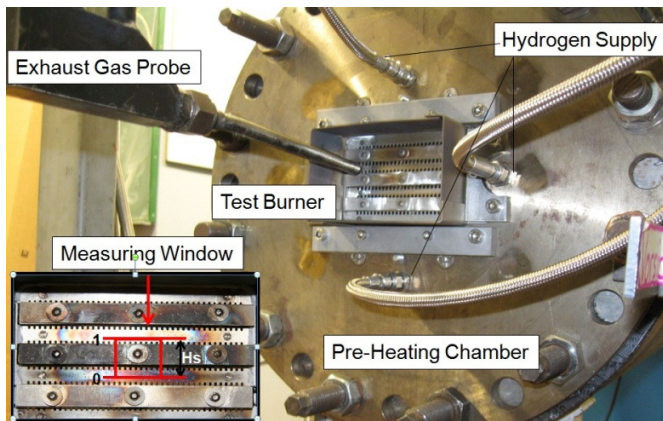


**Figure 3: Test burner mounted on test rig and measuring-window**

The ignition system is realized by a high voltage aircraft engine sparking plug which is always located on the same position during ignition procedure. After successful ignition of the burner the plug will be removed from hot exhaust gases. The test burner is equipped with flow metering units, pressure sensors and thermocouples for monitoring the operating conditions. A fully adjustable exhaust gas probe takes samples of the exhaust gases and is connected to exhaust gas analysis equipment. The measurements of the exhaust probe are located in a defined measuring-window (Figure 2 and 3) which covers representative phenomena of the combustion process. In the presented diagrams represents one data point the arithmetic mean value of the measuring points in the chosen measuring window. The term  $x/H_s$  specifies the vertical measuring position ( $x$ ) at the measuring window in relation to the general vertical size of the window ( $H_s=16\text{mm}$ ). This means that  $x/H_s=1$  is marginal above the hydrogen segment,  $x/H_s=0.75$  resides in the center of the segment,  $x/H_s=0.375$  is marginal under the hydrogen segment and  $x/H_s=0$  is arranged in the center of the air guiding panel.

## 5. EXPERIMENTAL INVESTIGATIONS

For the experimental characterization of the burning principle for higher energy densities, the investigation started by determining the ignition limits for each burner configuration. With regard of future gas turbine applications the ignition limits are determinate for part- and overload operational conditions. The ignition is tested at 50%, 75%, 100% and 110% air mass flow rate. The burner is regarded as ignited, if the ignition was audible and a rise of the exhaust gas temperature was detected. Figure 4a presents the ignition limits of the three burner configurations. In the diagram the relative required ignition energy is plotted against the equivalence ratio. The equivalence ratio is calculated by using the measured

hydrogen mass flow and the measured air mass flow during the ignition. The relative required ignition energy is the measured hydrogen mass flow multiplied by the constant net calorific value of hydrogen divided by theoretic applied heat release at the design point ( $\phi=0.4$ ). With increased energy density the ignition limit is shifted to lower equivalence ratios. In addition less ignition energy is required.

Figure 4b presents the operation capabilities of the tested burner configurations. In this diagram values of the burning efficiency are plotted against the equivalence ratio. The equivalence ratio and the burning efficiency are calculated from the measured exhaust gas emissions. The design point of the combustion principle is at  $\phi=0.4$ .

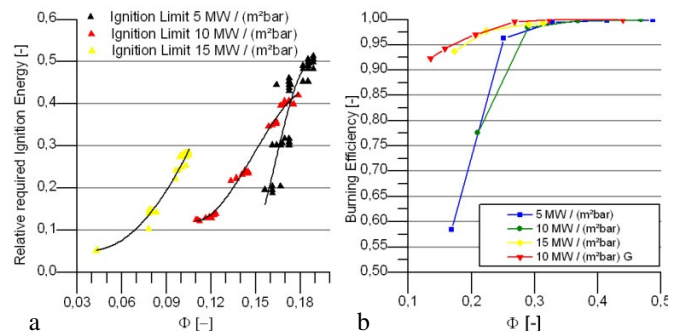


**Figure 4: Ignition limits and operation capabilities of the up scaled micromix burning principle**

In a wide range next to the design point the 5 MW- and the 10 MW-configuration reach 100% burning efficiency. In comparison the range of the 15 MW-burner is limited by the hot spot formation in front of the hydrogen segments at  $\phi>0.3$  because of the high thermal loading of the test burner material. For part load conditions the burning efficiency drops down. Although for part load conditions in all test burner configurations the impulse ratio and therewith air and hydrogen exit velocities are constant at the same equivalence ratios the resultant burning efficiency differs. The 10 MW-Gap-system shows wide operation stability, compared to the 10 MW-reference-configuration with the same jet in cross flow design parameter. The reason behind is that besides the jet in cross flow other flow phenomena have an important influence on flame positioning and anchoring influencing the burning efficiency. These phenomena will be discussed later on in detail.

Figure 5 shows the resultant  $\text{NO}_x$ -emissions against the equivalence ratio for the four different burner configurations. The presented  $\text{NO}_x$ -emissions are related to 15%  $\text{O}_2$ -content in the exhaust gas stream.

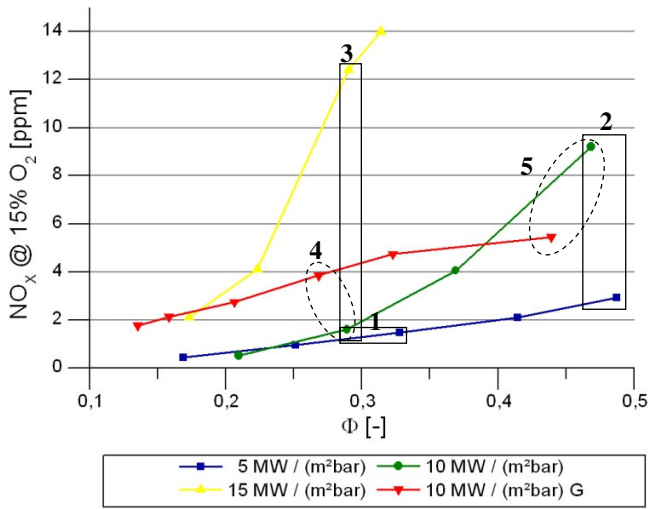


**Figure 5: Resultant NO<sub>x</sub>-emissions for different energy densities at T<sub>3</sub>=560 K p<sub>3</sub>= 1bar**

Both the 10 MW- and the 5 MW-burner show a similar NO<sub>x</sub>-characteristic at low equivalence ratios. At equivalence ratios higher than 0.3 the 10 MW-system, green line, shows a significant different behavior with increased NO<sub>x</sub>-emissions, while the 5 MW-reference system (blue line) shows its low NO<sub>x</sub>-formation behavior up to  $\phi=0.5$  as already known from former investigations [13]. An increase in the NO<sub>x</sub>-formation was expected due to the doubled energy density and the increased flame length due to the enhanced H<sub>2</sub>-injection hole diameter. But this sudden increase is driven by the flow phenomenon of “flame shifting” directing the H<sub>2</sub>-flames towards the hydrogen bars. The 15 MW-system with its three times higher energy density compared to the reference-system shows the same behavior but a steeper increase in NO<sub>x</sub>-emissions even at lower equivalence ratios.

The flow phenomenon influencing NO<sub>x</sub>-emissions is related to the recirculation zones surrounding and stabilizing the H<sub>2</sub>-flames. The burner geometry creates a system of several recirculation zones (Figure 2). One parameter for scaling to higher energy densities was also increasing the area and height of the air guiding panel gates by keeping the available space for the air guiding panels between two hydrogen segments constant (see Table 1). The scaling affects the distance between two gate-rows and reduces consequently the recirculation zones of the air guiding panels. This influences the flame position. During the investigations a shifting of the flame direction towards the H<sub>2</sub>-segments (Figure 6) was observed.

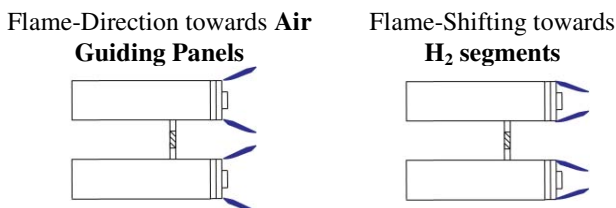


**Figure 6: Flame shifting**

With increased H<sub>2</sub>-mass flow, for both the 10 MW- and for the 15 MW-burner-configuration, the flames are directed towards the hydrogen segments with their related recirculation zones in the front of the segments. The flame reaction zone is therefore located in front of the hydrogen segments instead of between the shear layers of the recirculation zones of the hydrogen segments and air guiding panels. Unburned hydrogen enters into the recirculation zone and burns there. A zone of thermal loading, longer residence times and higher unmixedness is developed. As a consequence the resultant NO<sub>x</sub>-formation rises significantly.

In order to prove this theory exhaust gas measurements are compared and analyzed in chapter 5.1 for the different configurations and points of operation. For a better orientation boxes 1, 2, 3 in Figure 5 mark the compared configurations discussed in the following chapter 5.1.

In addition a different geometry configuration (Gap-system) was tested at 10 MW/(m<sup>2</sup>bar) (red line). Here in general increased NO<sub>x</sub>-emissions are measured at lower equivalence ratios. But at higher equivalence ratios the increase in NO<sub>x</sub>-emissions are even damped. The related additional flow phenomenon of “flame splitting” is discussed in chapter 6 comparing the two 10 MW-configurations at different points of operation (marked by the dotted circles 4, 5 in Figure 5).

## 5.1 FLAME ANCHORING INFLUENCING NOX FORMATION

In the following chapter the given theory provided for the rise of the NO<sub>x</sub>-formation will be substantiated with measured values. The Radial Temperature Distribution and the resultant NO<sub>x</sub>-emissions-profile of the measuring window for different flame positions at different equivalence ratios are compared with pictures of the flame positioning. The Radial Temperature Distribution is calculated as following:

$$RTDF = \frac{T_4 - T_{4\text{mean}}}{T_{4\text{mean}} - T_{3\text{mean}}} \quad (4)$$

In which T<sub>4</sub> is the local exhaust gas temperature at a measuring point calculated from the measured exhaust gas emissions, T<sub>4mean</sub> is the mean value of all measured values and T<sub>3mean</sub> is the mean value of the measured combustor inlet temperature.

For the different configurations and points of operations of the three boxes (1-3) plotted in Figure 5 the radial NO<sub>x</sub>-distribution and Radial Temperature Distribution are compared in Figure 7 and 8. The phenomenon of “flame shifting” influencing NO<sub>x</sub>-formation is visualized by pictures and related measurements for different burner configurations at comparable equivalence ratios. Figure 7 explains the sudden increase in NO<sub>x</sub>-formation of the 10 MW-system at higher equivalence ratios. Figure 8 shows the same phenomenon for the 15 MW-system at lower equivalence ratios.

For each point of operation (represented by a Box in Figure 5) two different burner configurations are compared. On the

left-hand side the RTDF and the  $\text{NO}_x$ -distribution is plotted against vertical measuring position in the chosen measuring window. For a better understanding sketches illustrate the prevailing flame position and the location of the measuring window. On the right-hand side pictures taken during the combustion process show the actual position of the  $\text{H}_2$ -flames. The pictures show the back end of the combustors; contrary to the flow direction (Figure 2). The viewing angle is about  $45^\circ$  from the center axis.

Flame shifting towards  $\text{H}_2$ -segments at higher energy densities enforces  $\text{NO}_x$ -formation:

The increase in  $\text{NO}_x$ -formation of 10 MW-burner compared to the 5 MW-burner is investigated by comparing points of operation of Box 1 and 2 in Figure 7. In Box 1 the 10 MW-burner is compared to the 5 MW-burner at  $\phi=0.3$ . Here both burner configurations have quite similar  $\text{NO}_x$ -emissions and no shifting of the flames takes place. Box 2 compares the temperature- and the  $\text{NO}_x$ -characteristic of these two burner configurations at a higher equivalence ratio of 0.47, when a shifting of the hydrogen flames towards the  $\text{H}_2$ -segments takes

place for the 10 MW-configuration.

At  $\phi=0.3$  flames of the 10 MW-burner do not shift towards the hydrogen segments. The highest temperatures of the 5 and 10 MW-burner are situated in front of the  $\text{H}_2$ -segment at  $x/\text{H}_s=0.75$  (Figure 7a). The development of the recirculation zones in front of the  $\text{H}_2$ -segment is visible. But due to the reduced energy density at low equivalence ratios no intensive  $\text{NO}_x$ -formation takes places (Figure 7b).

To visualize the flame position, Figure 7 contains photographic pictures (e-h) taken during the combustion. The blue hydrogen flames are clearly visible [21]. At  $\phi=0.3$ , for both configurations, no shifting of the  $\text{H}_2$ -flames is visible (Figure 7e, f).

For elevated equivalence ratios up to 0.47 in the 10 MW-configuration, the affection of the flame movement towards the segments is enforced. If the flames shift towards the hydrogen segments, the recirculation zones resulting from the  $\text{H}_2$ -segments are clasped by the hydrogen flames.  $\text{NO}_x$ -formation is established in this area due to the higher residence time and unmixedness of the reactants. This movement of the flames from the air guiding panels towards the  $\text{H}_2$ -segments is clearly

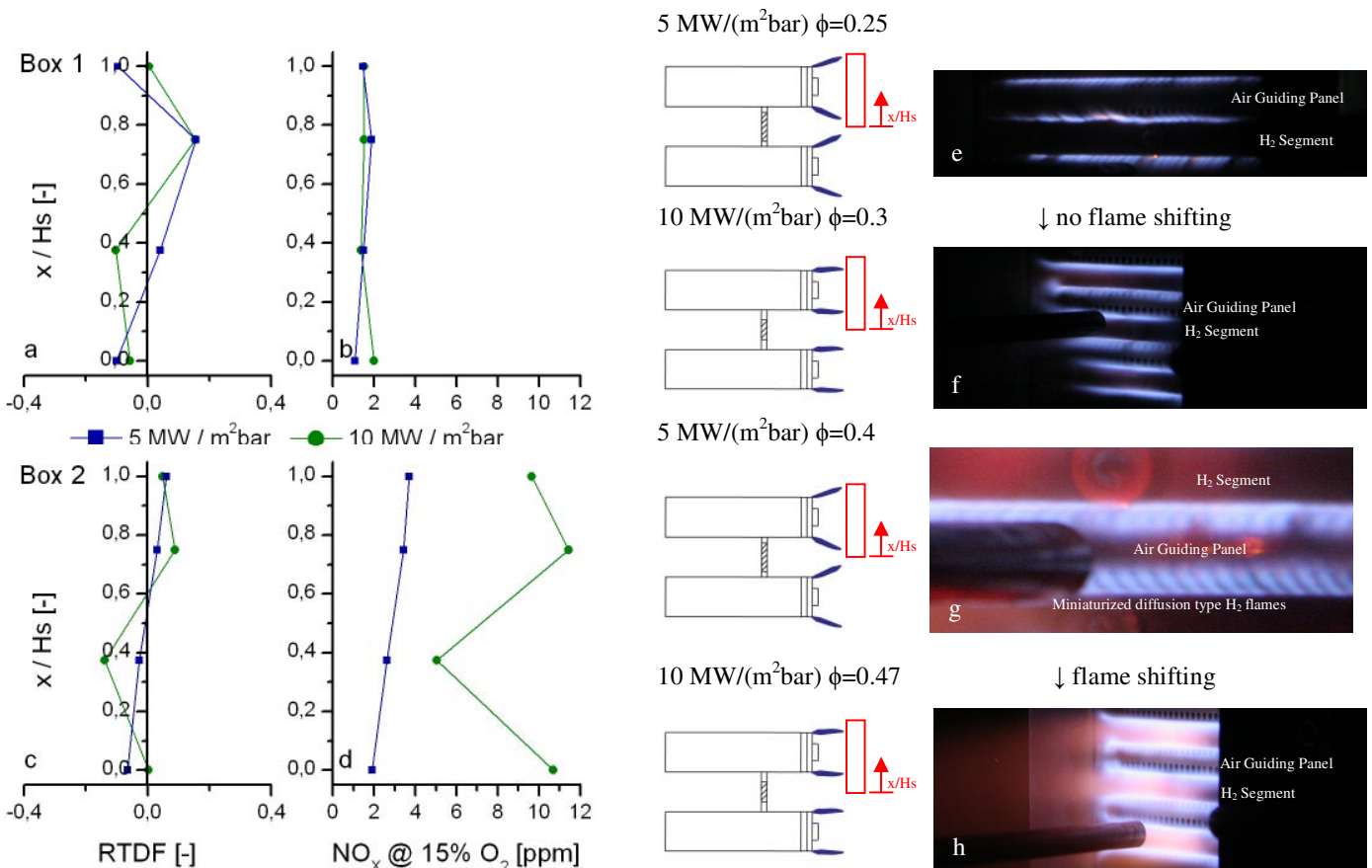


**Figure 7:** Flame shifting towards  $\text{H}_2$ -segments at higher energy densities enforces  $\text{NO}_x$ -formation 10 MW/( $\text{m}^2\text{bar}$ ) to 5 MW/( $\text{m}^2\text{bar}$ ) at  $\phi=0.3$  [a, b, e, f] and at  $\phi=0.47$  [c, d, g, h] at  $T_3=560 \text{ K}$   $p_3= 1\text{bar}$  (  $\square$  measuring window)



and mixture. For the 15 MW-configuration the maximum values of both the RTDF and the NO<sub>x</sub>-emissions are located in the zone in front of the hydrogen segments ( $x/H_s=0.75$ ). The enforced shifting of the flames at further increased energy density causes that the recirculation zone in front of the segment is the most dominant region where the combustion process takes place (Figure 8a+b). The resultant NO<sub>x</sub>-formation with increased hydrogen mass flow is not only enhanced by the increased residence time of the reactants but also by the higher prevailing temperature in this area.

## 5.2 AIR MASS FLOW VARIATION

The micromix combustion principle is planned for industrial gas turbine applications. Therefore the general part- and over-load operation is of interest. Also the rate of NO<sub>x</sub>-formation for the different mass flow variations has to be investigated. The 5 MW-reference-system is chosen for the mass flow investigations. For the mass flow variation the design momentum ratio remains constant but the velocities of the hydrogen and air jet change. With regard to the start up process of gas turbines the following mass flows are tested: 50%, 75% and 110% of the reference mass flow. The mass flow variations are done under the same experimental conditions used for the 100% reference mass flow case ( $T_3=560\text{K}$   $p_3=1\text{bar}$ ). Figure 9 shows the NO<sub>x</sub>-emissions reduced to 15% O<sub>2</sub> content in the exhaust gas stream against the equivalence ratio.

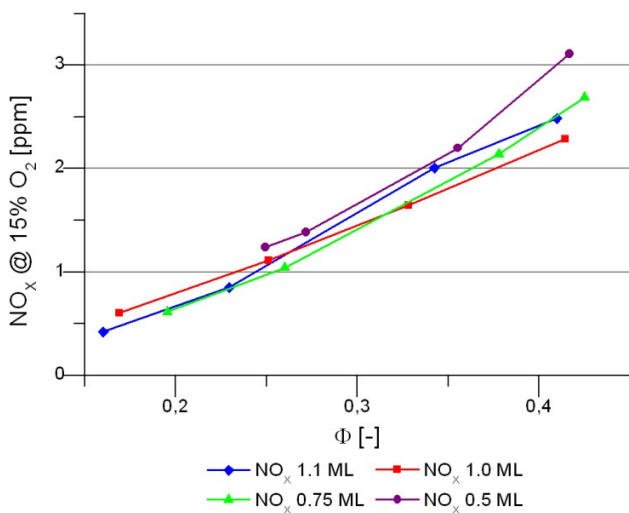


**Figure 9: Resultant NO<sub>x</sub>-emissions mass flow variation at  $T_3=560\text{ K}$   $p_3=1\text{ bar}$**

The system is capable of compensating significant changes in the air mass flow rate. The red line shows the NO<sub>x</sub>-emissions of the 100% air mass flow reference case. The NO<sub>x</sub>-emissions of the 75% and the 110% air mass flow have a similar NO<sub>x</sub>-formation characteristic. The emissions at 50% air mass flow rate are marginally higher. Based on this information and if the flame is well anchored between the layers, there appears to be no impulse influence on the formation of the NO<sub>x</sub>-emissions.

But regarding [15] where mixing is assumed to be a function of linear pressure drop and influences NO<sub>x</sub>-formation, a variation of impulse should have an influence on NO<sub>x</sub>-formation. For the micromix burning principle, there are other more dominant NO<sub>x</sub> influencing parameter. The micromix burning principle's low NO<sub>x</sub>-emissions results from the flame miniaturization with the number of local mixing zones increased in comparison to conventional gas turbine combustors. As a consequence the major influence parameter on the mixing process is the basic design philosophy of the combustion principle and the flame positioning between the recirculation zone layers, not the impulse.

## 6. OPTIMIZATION OF THE COMBUSTION PRINCIPLE AT HIGHER ENERGY DENSITY

Besides optimizing of the regular geometry of the micromix burning principle, a change in geometry can offer an improvement. The 5 MW-system shows low NO<sub>x</sub>-results. Therefore the 10 MW-burner-concept is chosen for further improvements of the burning principle. For the 5 MW-reference-configuration the dimension of the recirculation zones resulting from the hydrogen segments and from the air guiding panels are comparable. In order to prevent the H<sub>2</sub>-flames shifting towards the hydrogen segments resulting in an area of long residence time, the geometry of the air guiding panels is modified with regard to an equal distribution of the recirculation zones. By keeping all other design parameters constant a gap or silt instead of the gate configuration is used. The increased vertical distance between the air guiding panel gaps enlarges the resultant recirculation zones (Table 1 + Figure 2).

The investigations are carried out with the same procedure and conditions used during the former investigations. The red line in Figure 5 presents the resultant NO<sub>x</sub>-emissions against the equivalence ratio. In general the Gap-configuration is shifted to a higher NO<sub>x</sub>-formation compared to the 5 MW- and 10 MW-systems. But a rapid rise of the NO<sub>x</sub>-emissions at high equivalence ratios is avoided. In addition there is a damping effect on the rise of the NO<sub>x</sub>-emissions at high  $\phi$ -values. At  $\phi=0.47$  the resultant NO<sub>x</sub>-emissions are significant lower compared to 10 MW-reference case. The reason behind this is that the hydrogen jets are split and smaller H<sub>2</sub>-flames anchor on the segment and on the gap air guiding panels resultant in a doubled number of miniaturized flames (Figure 10).

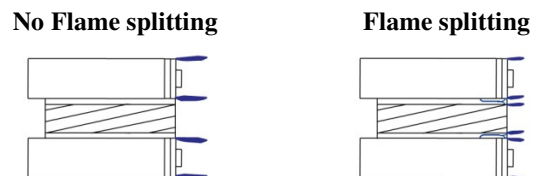


**Figure 10: Flame splitting**

For supporting this physical phenomenon of flame splitting, the gap air guiding panels are much thicker than the gate air guiding panels and create a kind of tunnel for the

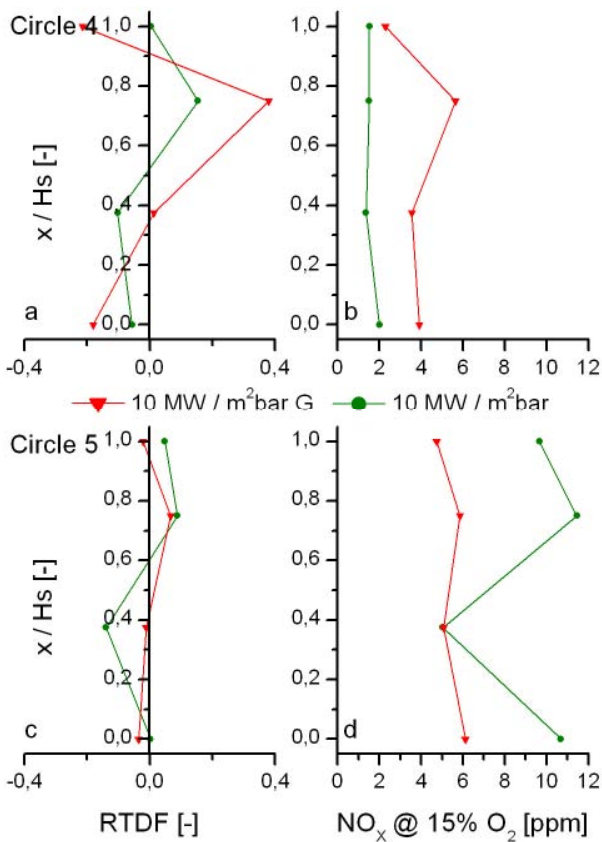


**Figure 11: Flame splitting lowering NO<sub>x</sub> at higher energy density 10 MW/(m<sup>2</sup>bar)-Gap to 10 MW/(m<sup>2</sup>bar) at  $\phi=0.3$  [a, b, e, f] and at  $\phi=0.47$  [c, d, g, h] at  $T_3=560\text{ K}$   $p_3=1\text{ bar}$  (□ measuring window)**

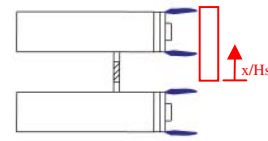
hydrogen injection. In addition the size of the gap is defined as the double injection depth ( $y$ ) of the hydrogen jets at the design point. The hydrogen is hence injected in the center of the air stream. This further miniaturizes the flames, thus a lower NO<sub>x</sub>-formation is achieved at elevated equivalence ratios.

For the different configurations and points of operations of the two dotted circles (4 + 5) plotted in Figure 5 the radial NO<sub>x</sub>-distribution and Radial Temperature Distribution are compared in Figure 11. The phenomenon of “flame splitting” influencing NO<sub>x</sub>-formation is visualized by pictures and related measurements for different burner configurations at comparable equivalence ratios in order to explain the damping effect on the rise of NO<sub>x</sub>-emissions of the 10 MW-Gap-system at higher equivalence ratios.

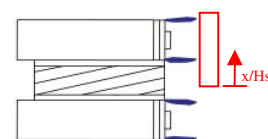
Flame splitting lowering NO<sub>x</sub>-emissions at higher energy density:

The different NO<sub>x</sub>-formation of 10 MW-Gap-burner compared to the 10 MW-reference-burner will be investigated in this section. In Circle 4 the 10 MW-Gap-burner is compared to the 10 MW-reference-burner at  $\phi=0.3$ . Here the gap burner has higher NO<sub>x</sub>-emissions and no splitting of the flames takes place. Circle 5 compares the temperature- and the NO<sub>x</sub>-

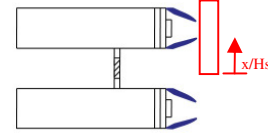
10 MW/(m<sup>2</sup>bar)  $\phi=0.3$



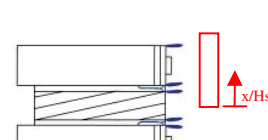
10 MW/(m<sup>2</sup>bar) Gap  $\phi=0.3$



10 MW/(m<sup>2</sup>bar)  $\phi=0.47$



10 MW/(m<sup>2</sup>bar) Gap  $\phi=0.47$



↓ no flame splitting

↓ flame splitting instead of flame shifting

characteristic of these two burner configurations at elevated equivalence ratio of 0.47, when a splitting of the hydrogen flames takes place for the 10 MW-Gap-configuration. Figure 11 presents the comparison of Circle 4 and Circle 5.

In Circle 4 at  $\phi=0.3$ , compared to the 10 MW-reference-system, the gap configuration has a higher NO<sub>x</sub>-formation in general and the splitting of the hydrogen flames does not take place. Compare also Figure 11e, f for this purpose. The elevated NO<sub>x</sub>-emissions, NO<sub>x</sub>-profile (Figure 11b), are originated by the non-optimized mixing capabilities of the Gap-configuration at lower equivalence ratios. At low equivalence ratios, the Gap-configuration has a reduced injection depth of the hydrogen. As consequence more unburned hydrogen enters in the recirculation zone in front of the H<sub>2</sub>-segment and burns there. The mixing characteristic of the reference system results in an uniform low NO<sub>x</sub>-distribution-profile. The flames of the Gap-configuration are directed towards to the air guiding gap panels. But the maximum exhaust temperatures are located at  $x/H_s=0.75$  (Figure 11a). Also in this case the distribution of the NO<sub>x</sub>-emissions follows the RTDF.

At  $\phi=0.47$  for the 10 MW-Gap-system the flames are split and further miniaturized H<sub>2</sub>-flames anchor on the hydrogen segments and on the gap air guiding panels (Figure 11h). The

flames of the 10 MW-reference configuration are shifted towards the hydrogen segments (Figure 11g), as discussed in Figure 7. Through the further miniaturization of the flames for the Gap-configuration a general lowering of the NO<sub>x</sub>-formation is achieved. Areas with circulated unburned hydrogen, resulting in increased NO<sub>x</sub>-emissions, are avoided. Therefore the NO<sub>x</sub>-distribution profile is more equable compared to the reference burner (Figure 11d). This fact is reflected in the Gap-burner's Radial Temperature Distribution, too (Figure 11c). Compared to Figure 11a the overall divergence is significantly reduced.

## 7. CONCLUSION AND OUTLOOK

During the investigations the ability of the micromix combustion principle to higher energy density industrial gas turbine applications up to 15 MW/(m<sup>2</sup>bar) was tested. For the experimental investigation tree test burners, 5, 10 and 15 MW/(m<sup>2</sup>bar), were used. Ignition- and extinction-limits and part load behavior are tested on the atmospheric test rig. The combustion principle offers wide operation range capabilities for secure and efficient hydrogen combustion in industrial gas turbine applications with a total pressure drop of the combustion chamber of less than 3%. Also for part- and over load conditions the qualification of the principle is proven. Compared to conventional industrial gas turbine combustors the micromix combustion principle offers a NO<sub>x</sub>-reduction potential by miniaturization of the H<sub>2</sub>-flames.

During the combustion process the flow phenomenon of "flame lifting" influences essentially the flame position and anchoring and therewith the resultant NO<sub>x</sub>-formation at higher energy densities. By scaling the geometry to higher energy densities the formation of the resultant recirculation zones in front of the air guiding panels are reduced. As consequence the recirculation zones in front of the H<sub>2</sub>-segments dominate the flame anchoring. The H<sub>2</sub>-flames shift towards the hydrogen segments. The reaction zone is more located in front of the segments instead of between the shear layers for the 5 MW-reference-system. Unburned hydrogen enters into the recirculation zone and burns there. A zone of thermal loading, longer residence times and higher unmixedness is developed. As a consequence the resultant NO<sub>x</sub>-formation rises significantly.

As learned from the 10 MW-reference-configuration the NO<sub>x</sub>-formation is not only controlled by the temperature distribution. Although a comparable temperature distribution is given at the same mean temperature, the NO<sub>x</sub>-distribution is significantly different. For the micromix burning principle the NO<sub>x</sub>-formation is mostly dominated by ideal position of the reaction zone between the shear layers. At further increased energy densities this effect gets more dominant.

By changing the geometry to an optimized gap-system for the 10 MW-burner the operational capability of the combustion principle is significantly increased. In general the resultant NO<sub>x</sub>-emissions are higher than for the reference configuration at lower equivalence ratios. But with increased equivalence ratio the second investigated flow phenomenon of "flame spitting" has an impact on the resultant NO<sub>x</sub>-formation. The

further splitting and miniaturization of the flames lowers the rise of the NO<sub>x</sub>-emissions at elevated equivalence ratios. This highlights further optimization potential of the micromix burning principle for low NO<sub>x</sub> hydrogen fuelled industrial gas turbine applications.

## ACKNOWLEDGMENTS

The presented work is accrued from the cooperation of the Siemens AG and the Aachen University of Applied Sciences. The Aachen University of Applied Sciences expresses its gratitude for the continuous help and advice of the Siemens AG during the research activities.

## NOMENCLATURE

$r_m$	[-]	momentum ratio
$\rho$	[kg/m <sup>3</sup> ]	density
$\eta_A$	[-]	burning efficiency
$u_j$	[m/s]	mean H <sub>2</sub> jet velocity
$u_\infty$	[m/s]	mean Air jet velocity
$d_{H_2}$	[m]	diameter of the H <sub>2</sub> injection hole
$y_{max}$	[m]	max. H <sub>2</sub> jet penetration
$z$	[m]	distance H <sub>2</sub> injection hole to combustion chamber angle
$x_{H_2}$	[m]	distance H <sub>2</sub> injection hole to air guiding panel
$\Phi$	[-]	equivalence ratio
ED	[MW/m <sup>2</sup> bar]	Energy Density
$m_{H_2}$	[g/h]	hydrogen mass flow
$H_u$	[kJ/kg]	constant net calorific value
$A_{design}$	[mm <sup>2</sup> ]	combustion chamber area
$p_3$	[bar]	combustor inlet pressure
$H_s$	[mm]	height of the measuring window
$x/H_s$	[-]	measuring position in relation to the height of the measuring window
$T_3$	[K]	combustor inlet temperature
$T_4$	[K]	local exhaust gas temperature
$T_{4mean}$	[K]	mean local exhaust gas temperature
$T_{3mean}$	[K]	mean combustor inlet temperature
RTDF	[-]	Radial Temperature Distribution Factor

## REFERENCES

- [1] Hannig, F., Smolinka, T., Bretschneider, P., Nicolai, S., Krüger, S., Meißner, F., and Voigt, M., 2009, "Stand und Entwicklungspotential der Speichertechniken für Elektroenergie- Ableitung von Anforderungen an und Auswirkungen auf die Investitionsgüterindustrie" Work Performed under BMWi Award: 08/28, Final Report, Germany.
- [2] Fadok, J., 2007, "Advanced Hydrogen Turbine Development, Phase 1," Work Performed under DOE Award: DE-FC26-05NT-42644, Final Report.
- [3] Mulready, R. C., 1964, "Liquid Hydrogen Engines,"

- Technology and Uses of Liquid Hydrogen*, Pergamon Press, Oxford, pp. 149-170.
- [4] Friedman, R., Norgren, C.T., and Jones, R.E., 1956, "Performance of a short turbojet combustor with hydrogen fuel in a quarter-annulus duct and comparison with performance in a full-scale engine," Technical Report No. *NACA RM E56D16*, Lewis Flight Propulsion Laboratory, Cleveland, Ohio, United States.
- [5] Sosounov, V., and Orlov, V., 1990, "Experimental Turbofan Using Liquid Hydrogen and Liquid Natural Gas as fuel," AIAA 90-2421, *Proc. 26<sup>th</sup> Joint Propulsion Conference*.
- [6] Shum, F., J. Ziemann, J., 1996, "Potential use of hydrogen in air propulsion," *Euro-Québec Hydro-Hydrogen Pilot Project (EQHHPP)*, European Union, Contract No. 4541-91-11 EL ISP PC, Final Report.
- [7] Westenberger A., 2003. "Liquid Hydrogen Fuelled Aircraft – System Analysis, CRYOPLANE", Final Technical Report No. GRD1-1999-10014, to the European Commission.
- [8] Wu, J., Brown, P., Diakunchak, I. S., Gulati, A., Lenze, M., and Koestlin, B., 2007, "Advanced Gas Turbine Combustion System Development for High Hydrogen Syngas Fuels", ASME Paper No. 2007-GT-28337.
- [9] Bradley, T., and Fadok, J., 2009, "Advanced Hydrogen Turbine Development Update," ASME Paper No. 2009-GT-59105.
- [10] Therkelsen, P., Werts, T., McDonell, V., and Sameslsen, S., 2008, "Analysis of NO<sub>x</sub> formation in a hydrogen fueled Gas Turbine Engine," ASME Paper No. 2008-GT-50841.
- [11] Schefer, R.W.; Smith, T. D.; and Marek, C.J.; 2003, "Evaluation of NASA Lean Premixed Hydrogen Burner," Technical Report No. SAND2002-8609 Sandia National Laboratory, United States.
- [12] Dahl, G., and Suttrop, F., 1998, "Engine Control and Low-NO<sub>x</sub> Combustion for Hydrogen Fuelled Aircraft Gas Turbines," *International Journal of Hydrogen Energy*, **23**(8), pp. 695-704.
- [13] Funke, H. H.-W., Boerner, S., Robinson, A., Hendrick, P., and Recker, E., 2010, "Low NO<sub>x</sub> H<sub>2</sub> combustion for industrial gas turbines of various power ranges," ETN-2010-42, *Proc. of the 5<sup>th</sup> International Conference the Future of Gas Turbine Technology*, Brussels, Belgium.
- [14] Goswami, M., Volkov, E. N., Konnov, A. A., Bastiaans, R.J.M., de Goey, L.P.H., 2010, "Updated Kinetic Mechanism for NO<sub>x</sub> Prediction and Hydrogen Combustion," *Low Emission Gas Turbine Technology for Hydrogen-rich Syngas*, European Union, Contract No. FP7-Energy-2008-Tren-1, Milestone-Report M2.2, University of Technology Eindhoven, The Netherlands.
- [15] Lefebvre, A. H.; 1984. "Fuel Effects on Gas Turbine Combustion-Liner Temperature, Pattern Factor, and Pollutant Emissions", *AIAA Journal of Aircraft*, **21**(11), pp 887-898.
- [16] Heywood, J.B., and Mikus, T., 1973, "Parameters controlling nitric oxide emissions from gas turbine combustion," Technical Report No. *AGARD-CP-125*, Massachusetts Institute of Technology, Cambridge, Massachusetts, United States.
- [17] Ziemann, J. et al. 1998. "Low NO<sub>x</sub> combustors for hydrogen fueled aero engine," *International Journal of Hydrogen Energy*, **23**(4), pp 281-288
- [18] Recker, E., Hendrick, P., Boerner, S., and Funke, H. H.-W., 2009, "Flow and application to the "Micromix" hydrogen combustion," ISABE-2009-1309, *Proc. 19th International Symposium on Air Breathing Engine*, Montreal, Canada.
- [19] Davis, T.W., and Beér, J.M., 1971. "Flow in the wake of Bluff-Body flame stabilizers," *Symposium (International) on Combustion*, **13**(1), pp 631-638.
- [20] Funke, H. H.-W., Robinson, A.E., Wagemakers R., and Hendrick, P., 2010, "Design and Testing of a Micromix Combustor with recuperative Wall Cooling for a Hydrogen Fuelled y-scale Gas Turbine", ASME Paper No. 2010-GT-23453.
- [21] Schefer, R.W., Kulatilaka, W.D., Patterson, B.D., and Settersten, T.B., 2009, "Visible emission of hydrogen flames," *Combustion and Flame*, **156**, pp 1234-1241.